

## Supporting information

### Pyridine caused structural reconfiguration forming ultrathin 2D metal-organic frameworks for oxygen evolution reaction

Yang Liu, †\* Shuwei Deng, † Shihui Fu, Xiaoteng Wang, Gang Liu and Haidong Yang, \*

#### Materials

Cobalt nitrate ( $\text{Co}(\text{NO}_3)_2 \cdot 6\text{H}_2\text{O}$ , >99% w/w) and potassium hydroxide (KOH, >98% w/w) were purchased from Anergy Chemical & 3A (Anhui Zesheng Technology Co., Ltd.). N,N dimethylformamide (DMF, >98% w/w), ferrous chloride tetrahydrate ( $\text{FeCl}_2 \cdot 4\text{H}_2\text{O}$ , >99% w/w) and 1,4-benzene dicarboxylic acid ( $\text{H}_2\text{BDC}$ , >98% w/w) were purchased from Sinopharm Chemical Reagent Co., Ltd. Pyridine (>99.5% w/w) and acetonitrile (MeCN, >98% w/w) was purchased from Shanghai Aladdin Biochemical Technology Co., Ltd. 1,4-diazabicyclo [2.2.2] octane (DABCO, >98% w/w) was purchased from Shanghai Macklin Biochemical Technology Co., Ltd. Ethanol was purchased from Lianlong Bohua (Tianjin) Pharmaceutical & Chemical Co., Ltd. Nafion was purchased from Suzhou Yi long sheng Energy Technology Co., Ltd. All aqueous solution was prepared by ultrapure water ( $\geq 18 \text{ M}\Omega \text{ cm}$ ) of the Millipore system. All reagents used in the experiment are analytical and have not been further purified.

#### Characterization

The crystal structure was characterized by X-ray diffraction with Cu K $\alpha$  radiation

( $\lambda = 1.5405 \text{ \AA}$ , Rigaku Ultima IV). The morphology was recorded with a Regulus field emission scanning electron microscopy (SEM, Ultra Plus, Carl Zeiss, Germany). The selected area electron diffraction (SAED) and energy-dispersive spectroscopy (EDS) mapping were performed on a FEI Tecnai F30 Super Twin TEM. Fourier-transform infrared (FT-IR) spectra were recorded for KBr-diluted samples using a Nicolet Nexus 670 IR spectrometer at wavenumbers of 400 to  $4000 \text{ cm}^{-1}$ . The thickness of MOF was measured with a DIMENSION ICON atomic force microscope (AFM). Thermogravimetric (TG) data was collected with a Shimadzu DTG-60A instrument at a heating rate of  $10 \text{ }^{\circ}\text{C}/\text{min}$  in nitrogen Gas. XPS data were recorded at an ESCALAB 250Xispectrometer with Al  $\text{K}\alpha$  x-ray spectrum (1486.6 eV).

The metal content of samples was quantitatively analyzed by inductively coupled plasma-optical emission spectroscopy (ICP-OES). 0.0068 g of solid sample was weighed and dissolved in a 50 mL volumetric bottle with  $\text{HNO}_3$  and then heated by microwave irradiation (Milestone, MLS-1200 MEGA, equipped with TFM inner vessels) until the solid was completely dissolved. The carbon lines were then calibrated by ICP-OES analysis with Agilent 5800 and JY 2501 monochromators (equipped with a spectral range of 175-785 nm). After continuously purging the optical path with nitrogen (2 L/min), calibration was performed with a 10%  $\text{HNO}_3$  standard solution at six different metal concentrations ( $0.001 \text{ mg mL}^{-1}$  to  $0.5 \text{ mg mL}^{-1}$ ). Data collection and processing were performed using ICP JY v 5.4.2

software (Jobin Yvon).

### **Electrochemical measurement**

The electrochemical measurements were performed at room temperature using an electrochemical workstation (CHI 660E, Shanghai C&H Instruments Co., Ltd.).

A standard three-electrode system was used for the tests, with a glassy carbon electrode (GCE, 3 mm diameter, 0.285 mg cm<sup>-2</sup> loading) as working electrode, graphite as counter electrode, and a saturated calomel electrode (3M KCl) as reference electrode. The working electrode was mechanically polished with Al<sub>2</sub>O<sub>3</sub> powder (Aldrich, 0.05 mm) and then washed with ethanol and deionized water, respectively. 4 mg of catalyst was dispersed in 1 mL of a 1:1 solvent mixture of water and ethanol containing 30 µL of Nafion (0.5 wt.%) solution and then sonicated for at least 30 min. 5 µL of the above well-dispersed solution (containing 20 µg of catalyst) was dropped onto the working electrode and dried at room temperature. Linear Sweep Voltammetry (LSV) curves were recorded at a scan rate of 5 mV s<sup>-1</sup>. The double-layer capacitance ( $C_{dl}$ ) value was operated by Cyclic Voltammetry (CV) at different scan rates (10-60 mV s<sup>-1</sup>) in a non-Faraday efficiency interval of 0.08 ~ 0.18 V vs. SCE. The Electrochemical Impedance Spectroscopy (EIS) was measured in the frequency range of 10<sup>6</sup>–10<sup>2</sup> Hz, 0.476 V vs. SCE amplitude of 5 mV s<sup>-1</sup>, and the experimental data were fitted. Tafel slope was calculated according to  $\eta = a + b \times \log j$ .<sup>1</sup> Here, a is a constant, b refers to Tafel slope,  $\eta$  is overpotential, and j is current density. The current

density was normalized to the geometrical surface area of the GCE ( $0.07\text{ cm}^2$ ).

And all potentials (vs. SCE) were converted to reversible hydrogen electrode (RHE) potential by the Nernst equation <sup>2</sup> ( $E_{\text{RHE}} = E_{\text{SCE}} + 0.059 \text{ pH} + E_{\text{SCE}}^\theta$ ,  $E_{\text{SCE}}^\theta = 0.242 \text{ V}$ ).

### **Single crystal structure determination**

Single crystal X-ray diffraction (SXRD) data of Co MOF-Py<sub>3</sub> were obtained on Bruker D8 VENTURE single crystal X-ray diffractometer at 298 K using Mo K $\alpha$  radiation ( $\lambda=0.71073 \text{ \AA}$ ). Crystal analysis was carried out on a PC using the Olex2 program to obtain all other non-hydrogen atom positions after obtaining some of them from the electron density distribution by the direct method, and the coordinates of all hydrogen atoms were obtained by geometric calculations and difference Fourier synthesis, and the coordinates of all non-hydrogen atoms and the anisotropic thermal parameter were corrected by the full-matrix least-squares method to convergence. Crystallographic data for Co MOF-Py<sub>3</sub> (2322052) can be obtained free of charge from The Cambridge Crystallographic Data Centre. All crystallographic and structure refinement data of Co MOF-Py<sub>3</sub> are presented in Table 1. Selected bond lengths and angles for Co MOF-Py<sub>3</sub> are given in Table S2.

**Table S1** The amount of  $\text{FeCl}_2 \cdot 4\text{H}_2\text{O}$  in different metal proportions.

$\text{Co}_x\text{Fe}_y\text{-Py}_3$ (x:y scale)	1:2	1:1	2:1	5:1	40:1
$n_{(\text{FeCl}_2 \cdot 4\text{H}_2\text{O})}$ (mmol)	1.44	0.72	0.36	0.144	0.018
$m_{(\text{FeCl}_2 \cdot 4\text{H}_2\text{O})}$ (mg)	286.3	143.1	71.6	28.6	3.57
DMF solution with $\text{FeCl}_2 \cdot 4\text{H}_2\text{O}$ (mL)	28.63	14.31	7.16	2.86	0.357

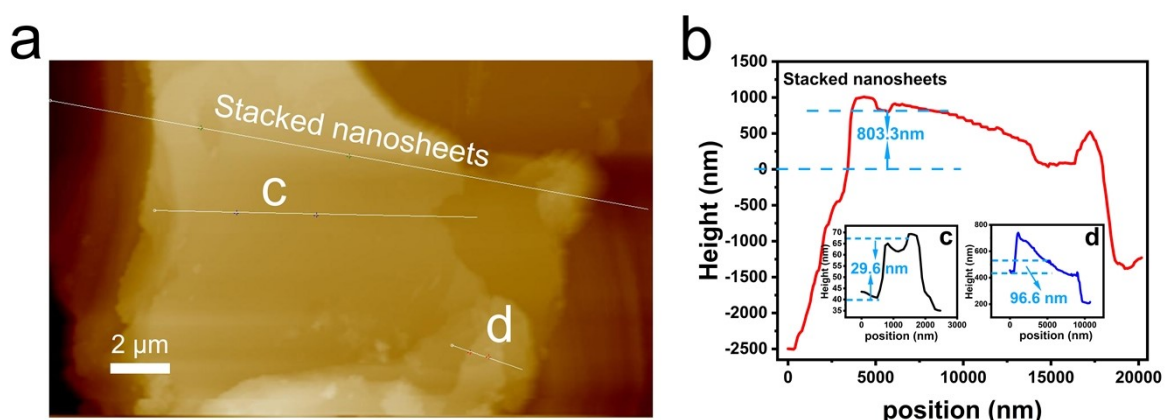


**Figure S1.** (a) AFM images of Co MOF-Py<sub>2</sub> nanosheets. (b) Measurement data of the nanosheet thickness in the underlined part of the AFM image.

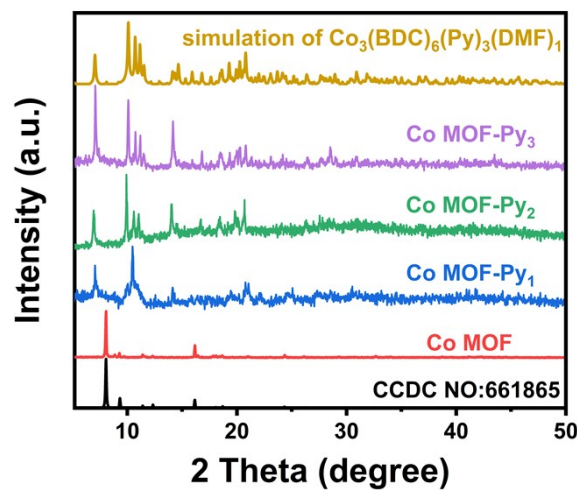


**Figure S2.** XRD patterns of a series of Co MOF-Py<sub>x</sub> (0, 1, 2, 3).

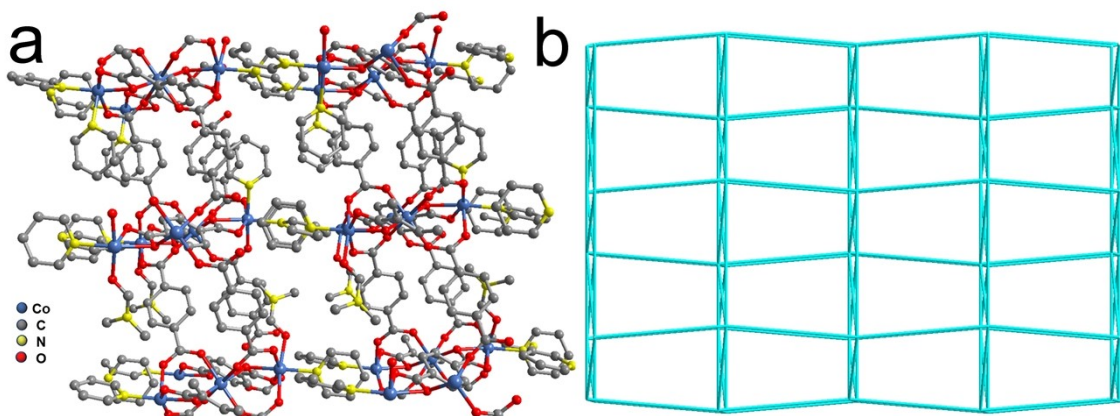


**Figure S3.** (a) Three-dimensional structure of Co MOF-Py<sub>3</sub>. (b) Three-dimensional topology of Co MOF-Py<sub>3</sub>.

**Table S2** Selected bond distances (Å) and angles (°) of Co MOF-Py<sub>3</sub>.

Co MOF-Py <sub>3</sub>			
Co1-O1#1	2.136(5)	Co3-O4#3	2.033(5)
Co1-O6#2	2.044(5)	Co3-O12	2.176(5)
Co1-O8#3	2.064(5)	Co3-O13	2.023(6)
Co1-O12	2.147(5)	Co3-O11	2.205(6)
Co1-O7	2.047(5)	Co3-O3	2.176(6)
Co1-O2#2	2.064(5)	Co3-N3	2.133(5)
Co2-O5	2.008(6)	Co2-O1#4	2.182(5)
Co2-C9#4	2.506(7)	Co2-O10	2.043(6)
Co2-N1	2.288(10)	Co2-O9#4	2.170(6)

---

Co2-N2	2.084(7)		
Co1-O6#2-O7	178.055(216)	Co2-N2-N1	90.614(367)
Co1-O6#2-O2#2	92.751(214)	Co2-O9#4-O1#4	60.075(223)
Co1-O6#2-O8#3	87.193(214)	Co2-O9#4-N1	87.172(342)
Co1-O6#2-O1#1	93.716(211)	Co2-O1#4-N1	85.557(335)
Co1-O6#2-O12	87.502(209)	O1-C9-Co1#5	134.301(459)
Co1-O7-O2#2	86.416(213)	O1-C9-Co2#2	89.259(427)
Co1-O7-O8#3	93.675(214)	O1-Co1#5-O9	137.172(300)
Co1-O7-O1#1	88.037(210)	O1-Co1#5-Co2#2	108.615(218)
Co1-O7-O12	90.790(209)	O1-Co1#5-C24	117.822(271)
Co1-O2#2-O8#3	178.844(210)	O1-Co1#5-H29#2	133.889(236)
Co1-O2#2-O1#1	89.543(205)	O1-O9-Co2#2	59.72(24)
Co1-O2#2-O12	93.347(202)	O1-Co2#2-C24	121.810(279)
Co1-O8#3-O1#1	89.308(195)	O1-Co2#2-H29#2	90.341(185)
Co1-O8#3-O12	87.804(195)	O4-C1-Co3#6	119.706(471)
Co1-O1#1-O12	176.808(193)	O4-Co3#6-O8	94.213(250)
Co3-O13-O4#3	98.373(224)	O4-Co3#6-C13	150.745(335)
Co3-O13-N3	87.414(238)	O6-C5-Co1#7	133.141(484)
Co3-O13-O12	100.117(205)	O6-Co1#7-O10	107.892(258)
Co3-O13-O3	172.617(248)	O6-Co1#7-C8	161.801(328)
Co3-O13-O11	93.478(238)	O6-Co1#7-H41	140.004(263)

---

Co3-O4#3-N3	101.974(235)	O8-C1-Co1#6	141.446(493)
Co3-O4#3-O12	98.077(201)	O8-Co#6-O4	121.001(271)
Co3-O4#3-O3	85.205(241)	O8-Co1#6-C13	148.862(315)
Co3-O4#3-O11	156.647(232)	O8-Co1#6-H33	112.005(220)
Co3-N3-O12	157.317(193)	O10-C5-Co2	133.500(495)
Co3-N3-O3	85.520(266)	O10-Co2-O6	106.710(264)
Co3-N3-O11	98.584(219)	O10-Co2-C8	167.971(336)
Co3-O12-O3	85.694(239)	O12-C26-Co1	129.774(455)
Co3-O12-O11	59.873(191)	O12-C26-Co3	90.366(425)
Co3-O3-O11	85.474(248)	O12-Co1-Co3	108.318(218)
Co2-O5-O10	96.348(227)	O12-Co1-O11	131.574(279)
Co2-O5-N2	101.661(245)	O12-Co1-C11	116.221(271)
Co2-O5-O9#4	156.954(252)	O12-Co3-O11	60.718(191)
Co2-O5-O1#4	99.050(204)	O12-Co3-C11	122.352(279)
Co2-O5-N1	81.127(312)	O13-C6-Co3	130.982(488)
Co2-O10-N2	86.515(244)	O13-Co3-O7	104.482(262)
Co2-O10-O9#4	96.361(257)	O13-Co3-C20	164.797(349)
Co2-O10-O1#4	98.275(203)	O13-Co3-H23	84.748(185)
Co2-O10-N1	175.729(315)	O7-C6-Co1	133.917(491)
Co2-N2-O9#4	98.231(279)	O7-Co1-O13	108.893(260)
Co2-N2-O1#4	158.088(250)	O7-Co1-C20	159.741(345)

O7-Co1-H25	140.027(261)	O5-Co2-C37	151.369(356)
O2-C15-Co1#7	140.243(496)	O5-Co2-H30	145.342(287)
O2-Co1#7-O5	118.673(271)	O11-C26-Co3	89.212(432)
O2-Co1#7-C37	151.161(327)	O11-C26-C11	32.644(422)
O2-Co1#7-H16	121.620(251)	O11-O12-Co3	59.409(189)
O9-C9-Co2#2	90.110(473)	O11-Co3-C11	121.205(294)
O9-Co2#2-O1	60.205(234)	O3-C12-Co3	117.828(684)
O9-Co2#2-C24	123.046(333)	O3-H12-Co3	91.976(296)
O5-C15-Co2	122.412(500)	O3-Co3-N4	146.971(477)
O5-Co2-O2	97.315(276)		

Symmetry transformations used to generate equivalent atoms:

#1 x, 1+y, z    #2 1-x, -0.5+y, 0.5-z    #3 1+x, y, z

#4 1-x, 1.5+y, 0.5-z    #5 x, -1+y, z    #6 -1+x, y, z

#7 1-x, 0.5+y, 0.5-z

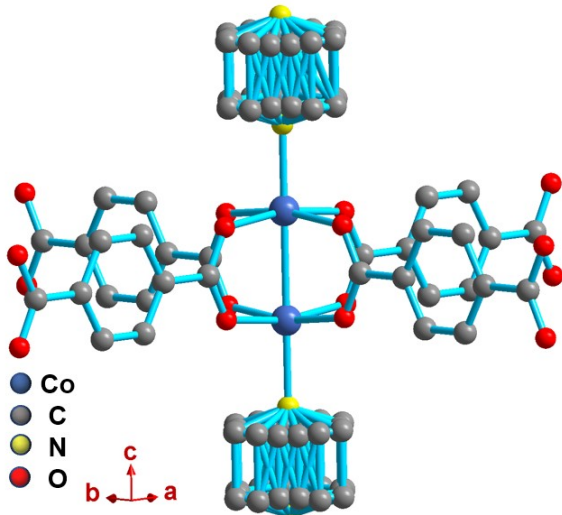


**Figure S4.** Coordination environment of  $\text{Co}_2(1,4\text{-BDC})_2(\text{DABCO})\cdot 4\text{DMF}\cdot \text{H}_2\text{O}$ .

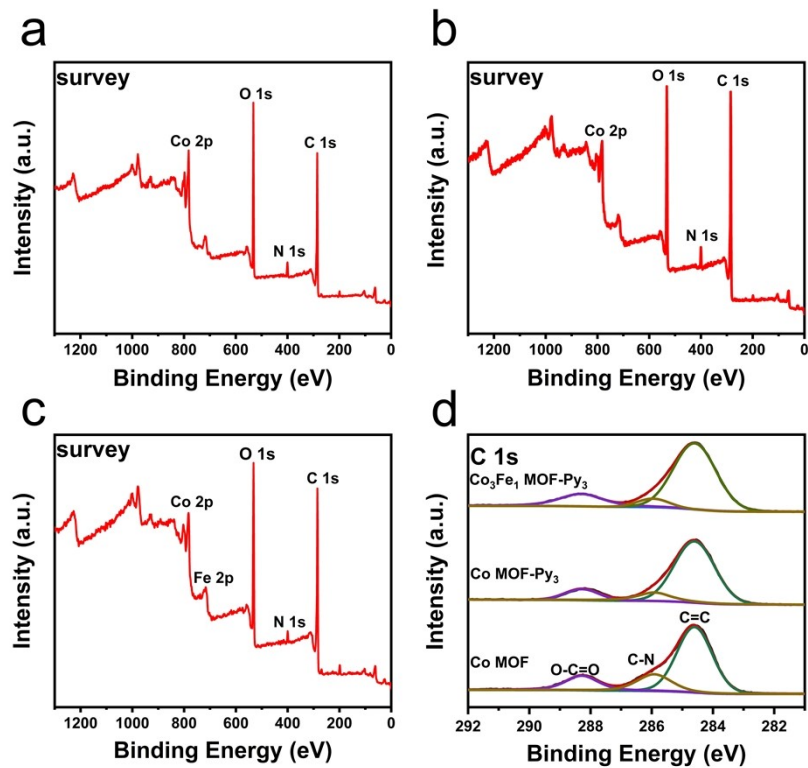


**Figure S5.** The full-scan XPS spectra of (a) Co MOF, (b) Co MOF-Py<sub>3</sub>, and (c) Co<sub>3</sub>Fe<sub>1</sub> MOF-Py<sub>3</sub>. (d) Deconvoluted high-resolution of C 1s.

**Table S3** The Co and Fe contents of Co<sub>3</sub>Fe<sub>1</sub> MOF-Py<sub>3</sub>.

Co	22.72%
Fe	7.19%
Co/Fe (molar ratio)	3.15:1

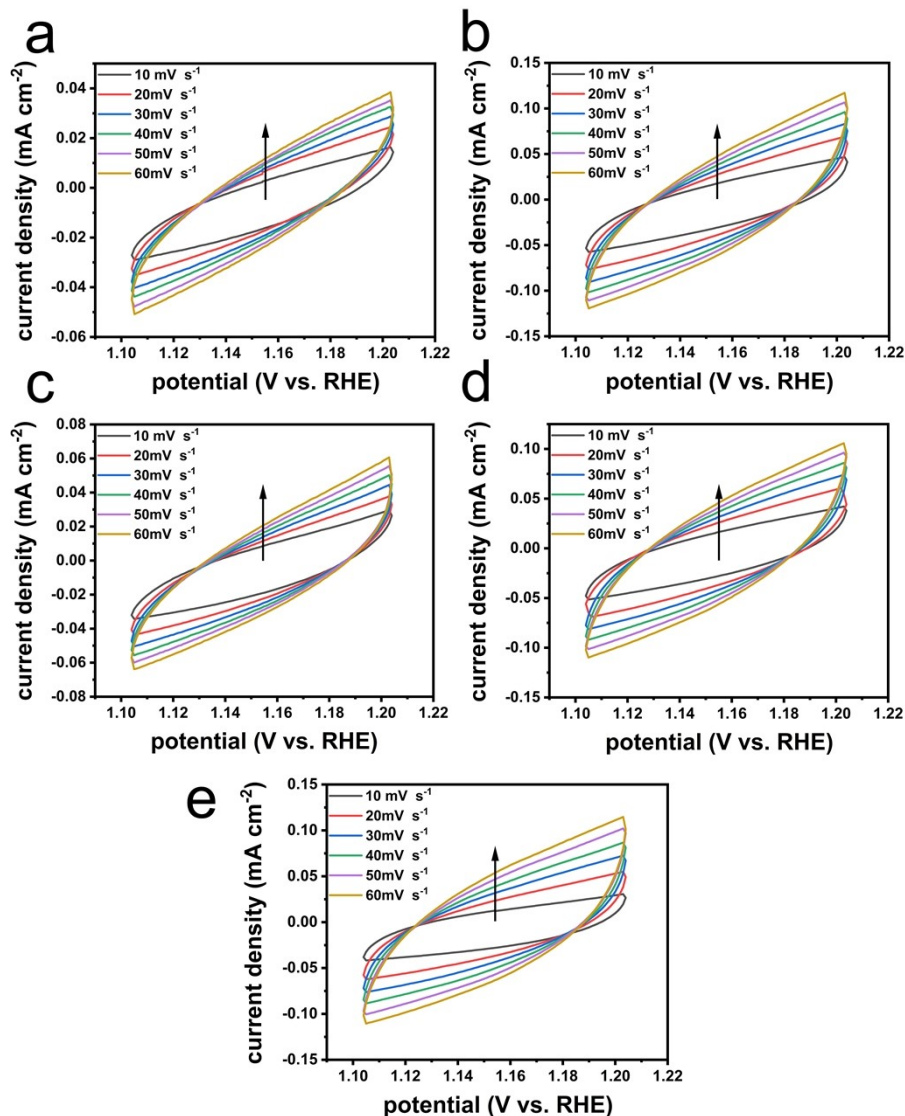


**Figure S6.** Cyclic voltammetry curves of (a) Co MOF, (b) Co MOF-Py<sub>1</sub>, (c) Co MOF-Py<sub>2</sub>, (d) Co MOF-Py<sub>3</sub>, and (e) Co<sub>3</sub>Fe<sub>1</sub> MOF-Py<sub>3</sub> at different scan rates from 10 to 60  $\text{mV s}^{-1}$ .

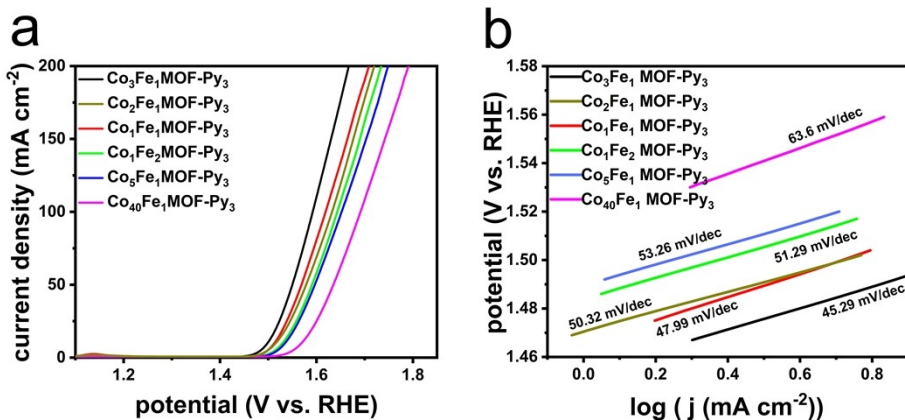


**Figure S7.** (a) LSV curves and (b) Tafel slope curves of a series of  $\text{Co}_x\text{Fe}_y$  MOF-Py<sub>3</sub>(x:y=1:2, 1:1, 2:1, 3:1, 5:1, 40:1).

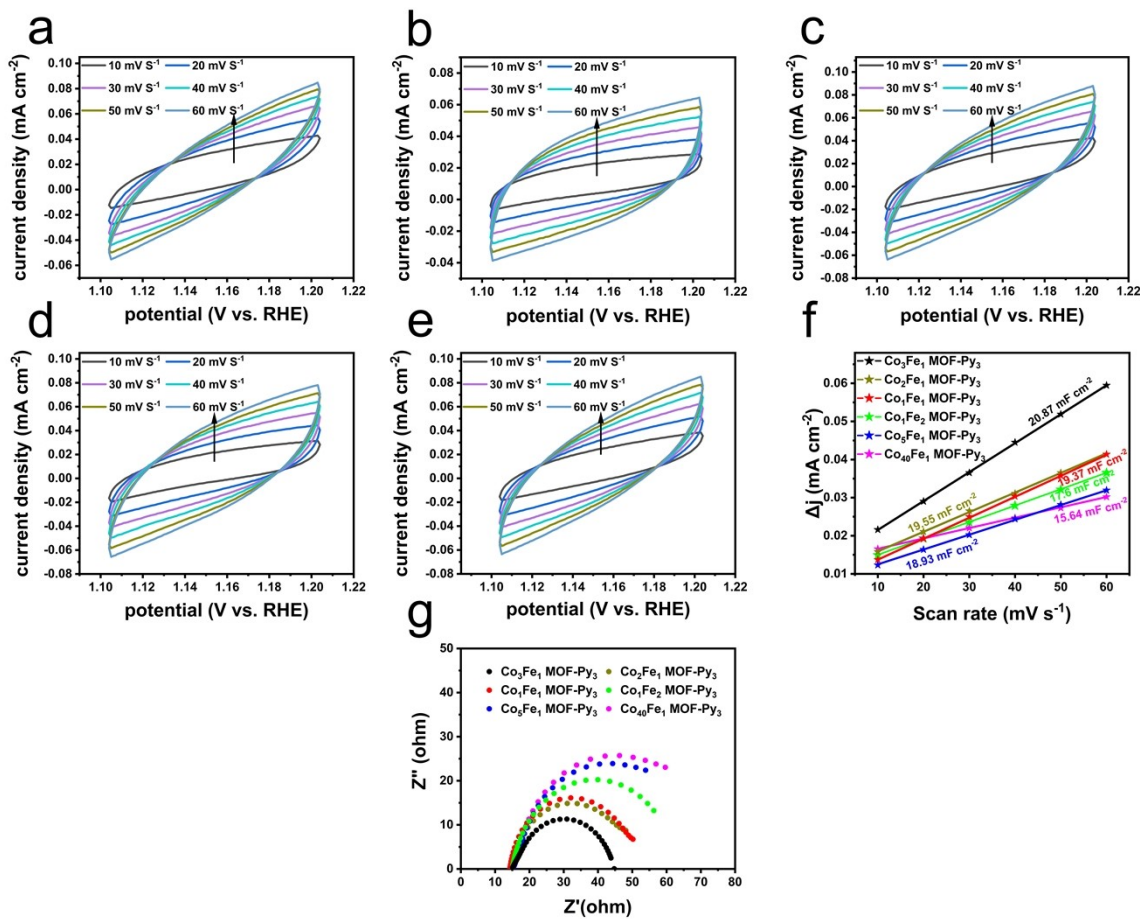


**Figure S8.** Cyclic voltammetry curves of (a)  $\text{Co}_1\text{Fe}_1$  MOF-Py<sub>3</sub>, (b)  $\text{Co}_2\text{Fe}_1$  MOF-Py<sub>3</sub>, (c)  $\text{Co}_1\text{Fe}_2$  MOF-Py<sub>3</sub>, (d)  $\text{Co}_5\text{Fe}_1$  MOF-Py<sub>3</sub>, (e)  $\text{Co}_{40}\text{Fe}_1$  MOF-Py<sub>3</sub>, (e) and

corresponding  $C_{dl}$  diagrams. (f) Nyquist plots of  $\text{Co}_3\text{Fe}_1$  MOF-Py<sub>3</sub>,  $\text{Co}_1\text{Fe}_1$  MOF-Py<sub>3</sub>,  $\text{Co}_2\text{Fe}_1$  MOF-Py<sub>3</sub>,  $\text{Co}_1\text{Fe}_2$  MOF-Py<sub>3</sub>,  $\text{Co}_5\text{Fe}_1$  MOF-Py<sub>3</sub>, and  $\text{Co}_{40}\text{Fe}_1$  MOF-Py<sub>3</sub> in 1 M KOH at a scan rate of 5 mV s<sup>-1</sup>.

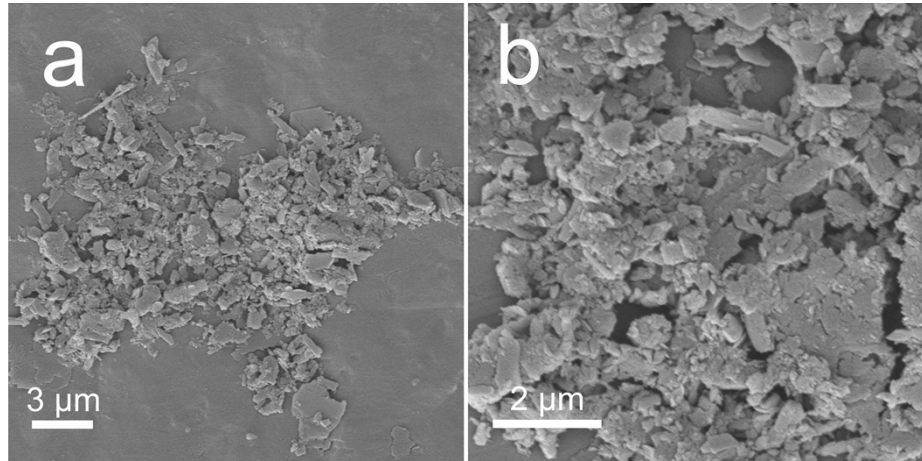


**Figure S9.** SEM images of  $\text{Co}_3\text{Fe}_1$  MOF-Py<sub>3</sub> catalyst after OER test.

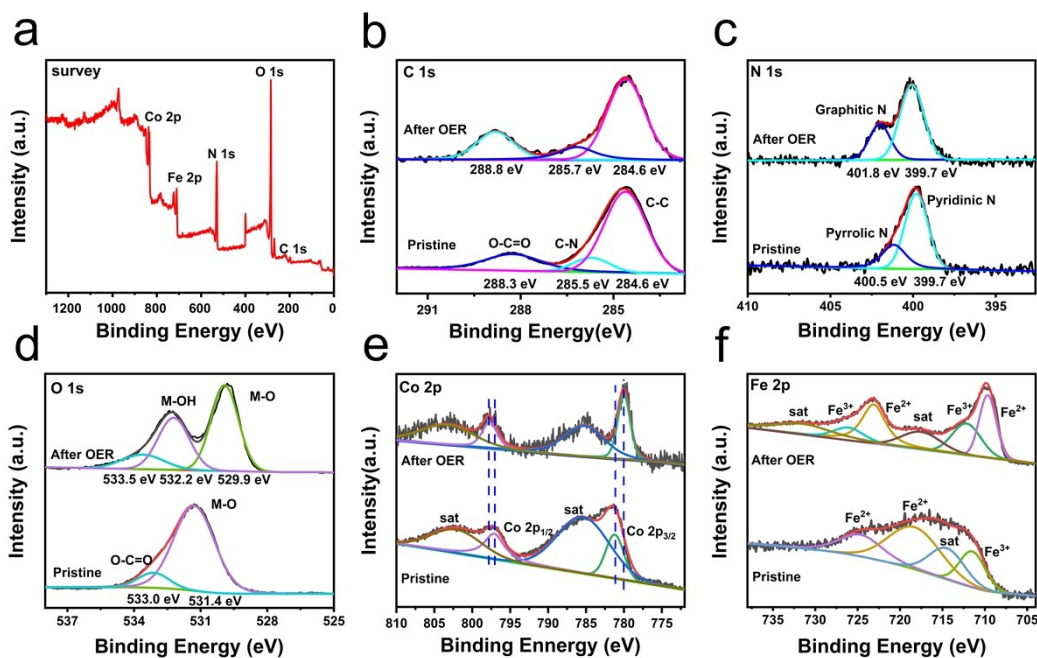


**Figure S10.** (a) The full-scan XPS spectra of  $\text{Co}_3\text{Fe}_1$  MOF-Py<sub>3</sub> after OER test.

Deconvoluted high-resolution XPS spectra of (b) C 1s, (c) N 1s, (d) O 1s 2p, (e) Co 2p, and (f) Fe 2p of  $\text{Co}_3\text{Fe}_1$  MOF-Py<sub>3</sub> after OER test.

**Table S4** Comparison of the OER activity of recently reported 2D MOF.

Catalysts	Mass	Tafel		Reference
	Loading (mg cm <sup>-2</sup> )	slope (mV dec <sup>-1</sup> )	$\eta_{10}$ (mV)	
CoMOF-Py <sub>3</sub>	0.285	52.14	307	This work
Co <sub>3</sub> Fe <sub>1</sub> MOF-Py <sub>3</sub>	0.285	42.59	269	This work
Co-SAC/RuO <sub>2</sub>	—	110	200	3
IrO <sub>2</sub>	0.26	57	288	4
PDA-MOF-0.1	0.249	66.1	350	5
Co BDC FcCA	—	53	280	6
Co Tp 3:1(Ni)	—	53.6	371	7
MOF 2	—	105	389	8
Co-MOF/Fe <sub>10</sub>	—	46.8	260	9
NiFe-2D MOF	2	56	260	10
Co/Ni (BDC) <sub>2</sub> TED	3	76.24	260	11
Cu Co MOF	—	118	380	12
Co <sub>3</sub> Fe-MOF	0.5	38	280	13
Fe@Co-BDC	0.5	34.1	307	14
Co Cu-MOF NBs	—	63.5	271	15
Ce@NiFe-MOF-5	—	54.55	258	16
Cu Co-MOF	—	173.5	340	17

Reference

1. Y. Wei, L. Yi, R. Wang, J. Li, D. Li, T. Li, W. Sun and W. Hu, *Small*, 2023, **19**.
2. K. Patil, P. Babar, D. M. Lee, V. Karade, E. Jo, S. Korade and J. H. Kim, *Sustainable Energy & Fuels*, 2020, **4**, 5254-5263.
3. K. Shah, R. Dai, M. Mateen, Z. Hassan, Z. Zhuang, C. Liu, M. Israr, W. C. Cheong, B. Hu, R. Tu, C. Zhang, X. Chen, Q. Peng, C. Chen and Y. Li, *Angewandte Chemie International Edition*, 2021, **61**.
4. Q. Deng, Y. Sun, J. Wang, S. Chang, M. Ji, Y. Qu, K. Zhang and B. Li, *Dalton Transactions*, 2021, **50**, 6083-6087.
5. F. Shi, Z. Wang, K. Zhu, X. Zhu and W. Yang, *Electrochimica Acta*, 2022, **416**.
6. F. He, Y. Zhao, X. Yang, S. Zheng, B. Yang, Z. Li, Y. Kuang, Q. Zhang, L. Lei, M. Qiu, L. Dai and Y. Hou, *ACS Nano*, 2022, **16**, 9523-9534.
7. S. Sprengel, M. Amiri, A. Bezaatpour, S. Nouhi, S. Baues, G. Wittstock and M. Wark, *Journal of The Electrochemical Society*, 2022, **169**.
8. A. Joshi, A. Gaur, P. Sood and M. Singh, *Inorganic Chemistry*, 2021, **60**, 12685-12690.
9. R. Yu, C. Wang, D. Liu, X. Wang, J. Yin and Y. Du, *Inorganic Chemistry*, 2022, **62**, 609-617.
10. Y. Liu, X. Li, Q. Sun, Z. Wang, W. H. Huang, X. Guo, Z. Fan, R. Ye, Y. Zhu, C. C. Chueh, C. L. Chen and Z. Zhu, *Small*, 2022, **18**.
11. D.-J. Li, Q.-H. Li, Z.-G. Gu and J. Zhang, *Journal of Materials Chemistry A*, 2019, **7**, 18519-18528.

12. J. Zhang, C. Zhang, X. Duo, Z. Liu, C. Liu, L. Guo, A. Xie and S. Luo, *Ionics*, 2020, **26**, 5123-5132.
13. W. Li, W. Fang, C. Wu, K. N. Dinh, H. Ren, L. Zhao, C. Liu and Q. Yan, *Journal of Materials Chemistry A*, 2020, **8**, 3658-3666.
14. W. Zhang, F. Li, Z. Fu, S. Dai, F. Pan, J. Li and L. Zhou, *Energy & Fuels*, 2022, **36**, 4524-4531.
15. W. Cheng, Z. P. Wu, D. Luan, S. Q. Zang and X. W. Lou, *Angewandte Chemie International Edition*, 2021, **60**, 26397-26402.
16. X. Wei, D. Liu, C. Wang, R. Yu, K. Zhang, S. Li, Z. Wu and Y. Du, *Inorganic Chemistry*, 2023, **62**, 3238-3247.
17. Q. Liu, J. Chen, F. Yu, J. Wu, Z. Liu and B. Peng, *New Journal of Chemistry*, 2021, **45**, 16714-16721.